Published in final edited form as:
J Hydrol (Amst). 2023 May ; 620: 1–9. doi:10.1016/j.jhydrol.2023.129432.

A temporally relaxed theory of physically or chemically non-equilibrium solute transport in heterogeneous porous media

Ying-Fan Lin[a], **Junqi Huang**[b], **Elliot J. Carr**[c], **Tung-Chou Hsieh**[d], **Hongbin Zhan**[e,*], **Hwa-Lung Yu**[a,*]

[a]Department of Bioenvironmental Systems Engineering, National Taiwan University, Taipei, Taiwan

[b]Groundwater Characterization and Remediation Division, Center for Environmental Solutions and Emergency Response, U.S. EPA, OK, USA

[c]School of Mathematical Sciences, Queensland University of Technology, Brisbane, Australia

[d]Disaster Prevention and Water Environment Research Center, National Yang Ming Chiao Tung University, Hsinchu, Taiwan

[e]Department of Geology and Geophysics, Texas A&M University, TX, USA

Abstract

Groundwater constitutes a critical component in providing fresh water for various human endeavors. Never-theless, its susceptibility to contamination by pollutants represents a significant challenge. A comprehensive understanding of the dynamics of solute transport in groundwater and soils is essential for predicting the spatial and temporal distribution of these contaminants. Presently, conventional models such as the mobile-immobile (MIM) model and the rate-limited sorption (RLS) model are widely employed to describe the non-Fickian behavior of solute transport. In this research, we present a novel approach to solute transport that is founded on the temporally relaxed theory of Fick's Law. Our methodology introduces two relaxation times to account for solute particle collisions and attachment, leading to the derivation of a new advection-dispersion equation. Our findings indicate that the relaxation times possess similar properties to the transport parameters in the MIM and RLS models, and our solution can be applied to accurately predict transport parameters from soil column experiments. Additionally, we discovered that the relaxation times are proportional to the magnitude of Peclet number. This innovative approach provides a deeper insight into solute transport and its impact on groundwater contamination.

[*]Corresponding authors: zhan@geos.tamu.edu (H. Zhan), hlyu@ntu.edu.tw (H.-L. Yu).

CRediT authorship contribution statement

Ying-Fan Lin: Conceptualization, Methodology, Software, Writing - original draft, Writing - review & editing, Visualization, Formal analysis. Junqi Huang: Methodology, Writing - review & editing. **Elliot J. Carr:** Methodology, Writing - review & editing. **Tung-Chou Hsieh:** Methodology, Writing - review & editing. **Hongbin Zhan:** Supervision, Writing - review & editing. **Hwa-Lung Yu:** Supervision, Writing review & editing, Project administration, Validation.

Declaration of competing interest

The authors declare that they have no known competing financial interests or personal relationships that could have appeared to influence the work reported in this paper.

Keywords

Temporally relaxed theory; Dual phase lag; Solute transport; Non-Fickian behavior; Anomalous transport; Sensitivity analysis

1. Introduction

Groundwater from aquifers constitutes a critical resource, however, contamination of this water source can have a severe impact on the subsurface environment and overall water security (Hillel, 2003). Water contained within porous media plays a vital role in sustaining plant growth and fulfilling human water demands. However, when contaminated by harmful or carcinogenic soluble components such as nitrates, pesticides, petroleum products, or heavy metals (Dracos, 1987; Addiscott et al., 1991; Miiler, 1996; Wood and Anthony, 1997), it can have devastating effects on the living conditions of our planet (Hillel, 2003). Thus, in order to develop effective strategies for groundwater and soil remediation, a comprehensive understanding of the mechanisms of contaminant fate and transport in aquifer systems is imperative (Bedient et al., 1994).

The advection-dispersion equation (ADE) is a commonly used tool in describing the fate and transport of contaminants in the environment. This equation presumes that the dispersive mass flux is governed by Fick's Law, which establishes a linear relationship between mass flux and concentration gradient. However, there are some complex physical and chemical processes that may be linked with the mass continuity equations, as recent research has demonstrated (Carr, 2020, 2021). Despite its widespread application, the conventional ADE, which is based on Fick's Law, can sometimes fall short in explaining observed concentration breakthroughs. This inadequacy is frequently attributed to the lack of consideration for non-Fickian behavior. Non-Fickian behavior, a topic that has been studied for several decades, refers to phenomena that do not conform to the linear relationship described by Fick's Law. Classical diffusion, related to Brownian motion and following Fick's Law, is characterized by a linear relationship between the mean squared displacement of a molecular particle and time (Benson et al., 2000, 2013; Edery et al., 2014; Kelly and Meerschaert, 2017). In contrast, anomalous transport displays a power-law correlation between the average squared displacement and time, resulting in a prolonged tailing of the concentration breakthrough curve.

This phenomenon is believed to arise from the influence of porous medium heterogeneity (Benson et al., 2000, 2013; Edery et al., 2014; Kelly and Meerschaert, 2017). Even in low Reynolds number systems, heterogeneous flow fields can significantly impact anomalous transport (Berkowitz et al., 2006, 2008). Ongoing research continues to unravel the complexities of non-Fickian behavior in contaminant transport.

The phenomenon of anomalous behavior in contaminants has been widely explored through various well-established theories (Kelly et al., 2017). These theories include the continuous-time random walk (Dentz and Berkowitz, 2003; Dentz et al., 2004; Berkowitz et al., 2006; Boano et al., 2007; Oliveira et al., 2021), two- or multiple-stage models (Brusseau et al., 1991; Gerke and Van Genuchten, 1993; Haggerty and Gorelick, 1995; Haggerty et al., 2000;

Huang et al., 2010; Malama et al., 2013; Huang and Goltz, 2015; Chen et al., 2019), and fractional ADEs (Benson et al., 2000, 2001; Berkowitz et al., 2002; Schumer et al., 2003; Benson et al., 2004; Zhang et al., 2007, 2009; Povstenko, 2015; Chen et al., 2017; Kelly and Meerschaert, 2017). The two-stage models, in particular, are noteworthy in simulating solute transport in media that exhibit mobile-immobile (MIM) zones and rate-limited sorption (RLS). The MIM model considers the transfer of solute mass between mobile and immobile zones, governed by first-order mass transfer kinetics. Similarly, the RLS model examines mass transfer between liquid and solid phases, also governed by first-order ratelimited kinetics. The MIM model is based on the explicit physical mechanism of water transfer between mobile pores and dead-end pores or between fractures and matrix blocks (Van Genuchten and Wagenet, 1989; Gao et al., 2010), while the RLS model allows for the simulation of chemical reactions such as absorption and adsorption (Huang et al., 2010). The model for transport in an aquifer-aquitard system (Brown et al., 2012; Huang and Goltz, 2015; Rezaei et al., 2016; Li et al., 2021) considers an aquitard located beneath or above a thin aquifer, with contaminant transport occurring in the highly permeable aquifer layer, and vertical diffusive mass transfer between the aquifer and aquitard. These models all take into account the micro- or macro-scale heterogeneity of porous media.

Intrinsic physical and chemical processes can play a major role in the fate and transport of contaminants, exhibiting time-dependent features such as concentration breakthrough retardation or tailing. The concept of time lags between mass flux and concentration gradient for Fick's law, known as "temporally relaxed theory", is inspired by the dual-phase lag model, which allows for heat flux and thermal gradient to occur at different times in Fourier's law (Tzou, 1995). This concept is motivated by the thermal wave behavior observed in pulse-laser experiments (Tzou et al., 1994). A similar concept can be found in well hydraulics known as lagging theory, which allows for water flow and hydraulic gradient to occur at distinct times in Darcy's law (Lin and Yeh, 2017; Lin et al., 2019). For instance, in a clay-rich formation, the well may start pumping at a constant rate but no water is abstracted from the clay, even though the hydraulic gradient occurs in advance. The "temporally relaxed theory" is used in this study to distinguish it from dual-phase lag and lagging theories.

The objective of this research is to modify Fick's law through the integration of the temporally relaxed theory, resulting in the creation of a novel ADE and a new model for non-Fickian transport. The theoretical analysis in this work reveals how the relaxation times relate to the intrinsic physical mechanisms that are traditionally governed by multiple equations and contain multiple parameters. The solution is derived using the Laplace transform technique, and a comparison of the present solution with the MIM and RLS models is carried out. In addition, a sensitivity analysis is performed to classify the importance of the transport parameters for the model. Finally, the present solution is used to perform parameter estimation by analyzing column experiments performed by Liang et al. (2018) and Li et al. (2009).

2. Methodology

2.1. Model setup

The distribution of solute concentration, $C\left[\mathrm{ML}^{-3}\right]$, can be described using the one-dimensional ADE given by:

$$R\frac{\partial C}{\partial t} = \frac{\partial}{\partial x}\left(-J\right) \tag{1}$$

where x is the distance from the source [L], t is the time [T], R is the retardation factor [-], and J is the mass flux $\left[\mathrm{ML}^{-2}\mathrm{T}^{-1}\right]$ induced by the dispersive and advective terms:

$$J\left(t\right) = -D\frac{\partial C(t)}{\partial x} + vC\left(t\right) \tag{2}$$

In Eq. (2), $D = \tau_0 D_0 + \alpha|v|$ is the dispersion coefficient $\left[\mathrm{L}^2\mathrm{T}^{-1}\right]$ and $v = q/n$ is the apparent velocity $\left[\mathrm{LT}^{-1}\right]$, where $\tau_0 \in [0,1]$ is the tortuosity [-], D_0 is the aqueous molecular diffusion coefficient $\left[\mathrm{L}^2\mathrm{T}^{-1}\right]$, α is the dispersivity [L], q is the Darcy flux $\left[\mathrm{LT}^{-1}\right]$, and n is the effective porosity. Typically, the influence of D_0 on the aggregate dispersion can be disregarded as its value is substantially smaller than $\alpha|v|$ in most situations.

Eq. (2) states that the mass flux and concentration gradient happen at the same time, implying that the speed at which the mass particles move is infinite. This assumption may not be accurate when there is an inertial force or structural interaction. Similar to the dual phase lag (Tzou et al., 1994) for Fourier's law or lagging theory (Lin and Yeh, 2017) for Darcy's law, Eq. (2) for Fick's law can be modified so that the mass flux and concentration gradient happen at different times.

$$J(t+\tau_J) = -D\frac{\partial C(t+\tau_C)}{\partial x} + vC(t+\tau_C) \tag{3}$$

Here, τ_J and τ_C are flux lagging and storage lagging [T] parameters, respectively. The flux lagging parameter, τ_J, reflects the relaxation time due to the inertial effect caused by the mass particle inertial collision, while the storage lagging parameter, τ_C, represents the relaxation time due to structural interactions such as sorption and secondary pore water interaction, see Fig. 1. When $\tau_J < \tau_C$, this means that the mass flux occurs earlier than the concentration gradient and that the flux is the cause of the gradient. If $\tau_J > \tau_C$, it implies that the mass flux is the result of the concentration gradient. For the case of $\tau_J = \tau_C$, the time lags are negligible, and Eq. (3) can be reduced to (2).

Assuming that τ_J and τ_C are quite small compared to the overall time t, the Taylor series expansion can be applied to Eq. (3), reading

$$\sum_{i=0}^{\infty}\frac{\tau_J}{i!}\frac{\partial^{i+1}}{\partial t^{i+1}}J\left(t\right)=\sum_{i=0}^{\infty}\frac{\tau_C}{i!}\frac{\partial^{i+1}}{\partial t^{i+1}}\left(-D\frac{\partial C(t)}{\partial x}+vC\left(t\right)\right) \tag{4}$$

Typically, the first-order approximation (i.e., truncating at = 1) is capable of capturing the major time lag effect on the concentration response. Following the work of Tzou (1995), Eq. (4) can be approximated by:

$$\left(1+\tau_J\frac{\partial}{\partial t}\right)J\left(t\right)\cong\left(1+\tau_C\frac{\partial}{\partial t}\right)\left(-D\frac{\partial C(t)}{\partial x}+vC\left(t\right)\right) \tag{5}$$

Substituting Eq. (5) into (1), the temporall relaxed ADE is then obtained as

$$R\left(1+\tau_J\frac{\partial}{\partial t}\right)\frac{\partial C}{\partial t}=\left(1+\tau_C\frac{\partial}{\partial t}\right)\left(\frac{\alpha q}{n}\frac{\partial^2 C}{\partial x^2}-\frac{q}{n}\frac{\partial C}{\partial x}\right),x\in\left[0,\infty\right) \tag{6}$$

or simplified as

$$R\left(1+\tau_C\frac{\partial}{\partial t}\right)\frac{\partial J}{\partial t}=\left(1+\tau_C\frac{\partial}{\partial t}\right)L_xC \tag{7}$$

where L_x is the spatial operator equal to $\left(\alpha q/n\right)\partial^2/\partial x^2-\left(q/n\right)\partial/\partial x$.

Assuming the porous medium is not contaminated initially, the associated initial conditions are given as

$$C(t=0)=\frac{\partial C(t=0)}{\partial t}=0 \tag{8}$$

When a tracer is introduced into a soil column, it may become diluted through mixing with water in the pre-inlet reservoir that does not contain the tracer. This can be mathematically described as (Wang et al., 2020; Shi et al., 2022):

$$V\frac{\partial C}{\partial t}\Big|_{x=0}=Aq(C_0(t)-C(x=0)) \tag{9}$$

where V is the volume of the cylindrical pre-inlet reservoir $\left[\mathrm{L}^3\right]$ and A is the cross-sectional area $\left[\mathrm{L}^2\right]$, with the injecting source $C_0\left(t\right)\left[\mathrm{ML}^{-3}\right]$ for two injection types:

$$C_0\left(t\right)=\begin{cases}\dfrac{M}{qA}\delta\left(t\right) & \text{for instantaneous pulse}\\ C_{in} & \text{for continuous injection}\end{cases} \tag{10}$$

where M is the mass of the solute injected into the medium [M], $\delta(t)$ is the Dirac delta function of time $\left[\mathrm{T}^{-1}\right]$, and C_{in} is the constant injection concentration $\left[\mathrm{ML}^{-3}\right]$.

A far field boundary condition is also imposed, which can be expressed as

$$\lim_{x \to \infty} C\left(x\right) = 0 \tag{11}$$

2.2. Semi-analytical solution

Applying the Laplace transform to Eqs. (6)–(11), the transformed equations are obtained as

$$R(1 + s\tau_J)s\bar{C} = (1 + s\tau_C)L_x\bar{C} \tag{12}$$

$$\mathrm{Vs}\,\bar{C}\left(x = 0\right) = Aq\left(\bar{C}_0\left(s\right) - \bar{C}\left(x = 0\right)\right) \tag{13}$$

with

$$\bar{C}_0\left(s\right) = \begin{cases} \dfrac{M}{qA} & \text{for instantaneous pulse} \\ \dfrac{C_{in}}{s} & \text{for continuous injection} \end{cases} \tag{14}$$

$$\lim_{x \to \infty} \bar{C}\left(x\right) = 0 \tag{15}$$

where the $\bar{C}$ represents the concentration function in the Laplace domain and s is the Laplace parameter. By introducing the Peclet number $Pe = vx/\alpha = x/\alpha$, Eq. (12) has a general solution expressed as

$$\bar{C} = c_1\exp\left(\frac{1 - \mu(s)}{2}Pe\right) + c_2\exp\left(\frac{1 + \mu(s)}{2}Pe\right) \tag{16}$$

with

$$\mu\left(s\right) = \sqrt{\frac{q(1 + s\tau_C) + 4nRs\alpha(1 + s\tau_J)}{q(1 + s\tau_C)}} \tag{17}$$

where c_1 and c_2 are undetermined coefficients. To satisfy the boundary conditions, the undetermined coefficients c_1 and c_2 are obtained, respectively, as $Aq\bar{C}_0\left(s\right)/\left(Aq + sV\right)$ and 0.

Inserting these expressions for c_1 and c_2 into Eq. (16), the semianalytical solution can then be derived as

$$\bar{C} = \frac{Aq\bar{C}_0\left(s\right)}{Aq + sV}\exp\left(\frac{1 - \mu(s)}{2}Pe\right) \tag{18}$$

Eq. (18) can be numerically evaluated using numerical Laplace inversion schemes such as the Stehfest (1970) algorithm and the Trefethen et al. (2006) algorithm (the associated

application to ADE can be found in previous works of Carr and Turner, 2016; Carr, 2020). Recently, Horváth et al. (2020) developed a numerical Laplace inversion scheme called the concentrated matrix-exponential (CME) method. Compared to the Gaver-Stehfest method (Gaver, 1966; Stehfest, 1970), Euler method rooted in Fourier series approximation (Dubner and Abate, 1968), and the Talbot method (Trefethen et al., 2006), the CME method has the best numerical stability, avoids overshooting and undershooting issues, and gains accurate results as the order used in the CME increases. Horváth et al. (2020) provided the code written in Mathematica, Matlab, and Python scripts, and the readers can get these codes for free in the GitHub repository at https://github.com/ghorvath78/iltcme. Here, we apply the CMS-S method (Horváth et al., 2023), an extending version of CMS method, to inverse our Laplace-domain solution.

2.3. Sensitivity analysis

To understand the impact of transport parameters on solute transport, we conduct a sensitivity analysis to evaluate the effect of parameter uncertainty on the system output (DellÓca et al., 2020; Knabe et al., 2021). We calculate the normalized sensitivity coefficients, X_k, which (Kabala, 2001) defines as:

$$X_k = \frac{\partial O}{\partial \ln(P_k)} = P_k \frac{\partial O}{\partial P_k} \tag{19}$$

where X_k represents the normalized sensitivity of the output O (i.e., concentration, C) to changes in the kth input transport parameter, P_k. We evaluate this at the observation point $x = 5$ cm in the time interval $t \in (0s, 1000s]$. Using the first-order forward or backward finite-difference formula to approximate the derivative in Eq. (19) only provides a first-order accurate estimate of the normalized sensitivity coefficients. Therefore, we adopt the three-point backward difference approach to improve the accuracy to second-order. This allows us to compute the normalized sensitivity coefficients using:

$$X_k \approx P_k \frac{3O(P_k) - 4O(P_k - \Delta P_k) + O(P_k - 2\Delta P_k)}{2\Delta P_k}, \tag{20}$$

where ΔP_k is a small differential change in the k th parameter, which we approximate by $10^{-3}P_k$ as suggested by Liou and Yeh (1997). We use the absolute values to rank the importance of the coefficients. A small magnitude of X_k indicates that large changes in the parameter P_k produce only small changes in the response or output variable O, indicating low sensitivity. This means that the parameter P_k would be difficult to estimate from the O measurements. It is also important to have linear independence among the sensitivity coefficients of the different parameters. Additionally, a positive value of X_k means that a small increase in P_k will result in an increase in concentration values, while a negative value of X_k indicates that a small increase in P_k will decrease concentration values.

3. Results

3.1. Comparison with two existing models

There are typically two classical two-stage models used to describe transport behavior. One is the MIM model, which is based on the assumption of physical non-equilibrium. In this model, solute particles are transferred between the mobile zone (e.g., fractures) and the immobile zone (matrix blocks). The other model is the RLS model, which reflects two-site sorption due to chemical non-equilibrium. In this model, solutes attach to soil particles through absorption or adsorption. A point to note is that although the MIM model and RLS model involve different non-equilibrium transport mechanisms (physical versus chemical), they are mathematically equivalent to each other. In this study, we will compare the MIM and RLS models with the temporally relaxed model, so we will discuss them in more detail below for convenience.

3.1.1. Mobile-immobile model—The ADEs derived based on the MIM concept for the mobile zone and the immobile zone can be written, respectively, as (Van Genuchten and Wagenet, 1989; Gao et al., 2010)

$$\beta R_m \frac{\partial C_m}{\partial t} + \left(1-\beta\right) R_{im} \frac{\partial C_{im}}{\partial t} = L_x C_m, x \in \left[0, \infty\right) \tag{21}$$

and

$$n_{im} R_{im} \frac{\partial C_{im}}{\partial t} = \omega (C_m - C_{im}) \tag{22}$$

where the subscripts m and im represent the mobile zone and immobile zone, respectively, $\beta = n_m/n$ and $(1-\beta) = n_{im}/n$, meaning that $n_m + n_{im} = n$, and ω is the first-order mass transfer rate coefficient $\left[\mathrm{T}^{-1}\right]$ between both continua. Substituting Eq. (22) into (21), the MIM ADE in terms of C_m is

$$\left(\frac{n_m}{n} R_m + \frac{n_{im}}{n} R_{im}\right)\left(1 + \frac{n_m R_m n_{im} R_{im}}{\omega (n_m R_m + n_{im} R_{im})} \frac{\partial}{\partial t}\right) \frac{\partial C_m}{\partial t} = \left(1 + \frac{n_{im} R_{im}}{\omega} \frac{\partial}{\partial t}\right) L_x C_m \tag{23}$$

3.1.2. Rate-limited sorption model—For the ADE derived from the RLS concept, the governing equations for the liquid phase and the solid phase can be written, respectively, as follows (Brusseau et al., 1991; Huang et al., 2010).

$$\frac{\partial C}{\partial t} + \frac{\rho_b}{n} \frac{\partial S}{\partial t} = L_x C, x \in \left[0, \infty\right) \tag{24}$$

and

$$\frac{\partial S}{\partial t} = \omega^* (k_d C - S) \tag{25}$$

where S is the mass amount in the solid phase [-], ρ_b is the bulk density of the porous medium $\left[\mathrm{ML}^{-3}\right]$, ω^* is the first-order mass transfer coefficient of sorption $\left[\mathrm{T}^{-1}\right]$, and k_d is the partition coefficient of adsorption $\left[\mathrm{M}^{-3}\,\mathrm{L}\right]$. Again, substituting Eq. (25) into (24), the RLS ADE in terms of C can be derived as

$$\left(1+\frac{\rho_b k_d}{n}+\frac{1}{\omega^*}\frac{\partial}{\partial t}\right)\frac{\partial C}{\partial t}=\left(1+\frac{1}{\omega^*}\frac{\partial}{\partial t}\right)L_x C \tag{26}$$

3.1.3. Physical meaning of τ_J and τ_C—Compared proposed ADE, Eqs. (6), to (23) and (26), we can find the relationships between the parameters in the temporally relaxed model and those in the MIM model and RLS model as listed in Table 1.

As table shown, the retardation factor, defined as $S = k_d C$, is the same for linear sorption. On the other hand, the relaxation times τ_J and τ_C are the reciprocal of the transfer rate coefficient multiplied by different constants. This means that an increase in ω or ω^* reduces the relaxation time values. By increasing the mass exchange rate between the primary and secondary pores for the MIM model or between the liquid and solid phases for the RLS model, the two-stage process is sped up until the solute transport can be accurately described by a classical ADE. This shows that the three models share the same two-stage process, but they cannot be used interchangeably due to their different concepts of the solute transport mechanism. The proposed method characterizes the two-stage process using two empirically determined relaxation times without the need for knowledge of the matrix blocks or sorption properties and their physical interactions with the system.

According to the model, the relaxation times, τ_J and τ_C, provide valuable information about particle collisions and attachment in porous media. An increase in τ_J is an indicator of a higher frequency of particle collisions, leading to an increase in particle inertia. On the other hand, a higher value of τ_C suggests a stronger sorption effect, hindering particle attachment to the soil.

It is important to consider the factors that impact the relaxation times when analyzing solute particles in porous media. For particle collisions, the causes may include concentration of the solute, porosity of the porous media, flow rate, environmental variables such as temperature or pressure, and fluid properties like water density and viscosity (McDowell-Boyer et al., 1986; Elimelech and O'Melia, 1990; Panfilov et al., 2008). For particle attachment, the factors that may play a role include surface charge of the solute particles, grain shape parameters, pore connectivity, surface area of the porous matrix, interfacial tension, chemical composition of both the solute and the matrix, and fluid properties such as friction forces (Bradford et al., 2002; Yang et al., 2022; Ogolo and Onyekonwu, 2022).

In order for particle collisions to occur, the concentration of solute particles in the porous media must be high, as more particles mean a greater likelihood of collision. A porous matrix provides more space for solute particles to move, leading to an increased chance of collision. The velocity and direction of fluid flow also impact collision frequency, as fast fluid flow can increase the velocity of solute particles and result in more frequent collisions.

Environmental factors like temperature and pressure can influence the velocity of the solute particles and increase the likelihood of collision. Finally, increased water density or viscosity leads to greater resistance to flow, causing more frequent collisions

For particle attachment, the electric charge on the solute particles affects their ability to adsorb onto the porous matrix. If the solute particles are charged, they may attract or repel each other, hindering attachment. The shape of the grains in the porous matrix also plays a role, as irregular shapes provide greater surface area for solute particles to adsorb onto. A well-connected pore network increases the likelihood of attachment by providing greater contact between the solute particles and the porous matrix. A larger surface area of the porous matrix can result in increased opportunity for solute particles to adsorb, while smaller surface area leads to decreased attachment. Interfacial tension between the solute particles and the porous matrix affects attachment, as does the chemical composition of both the solute and the matrix. Finally, changes in fluid properties such as friction forces can impact the mobility of the solute particles, increasing their likelihood of attachment.

While it may be difficult to mathematically link these factors to the relaxation times using the present model, understanding their impact provides a clearer picture of the potential causes of the observed relaxation times.

3.2. Effects of relaxation times

In this section, we focus on the impact of the parameters τ_J and τ_C on the concentration distribution. As shown in Fig. 2, changing the values of these parameters affects the temporal concentration curves for both (a) an instantaneous pulse and (b) continuous injection. The default values for $R, q, n, A, \alpha, M, C_{in}, \tau_J, \tau_C$, and observed point x are set as $1, 10^{-5}$ m/s, $0.2, 0.025^2\pi\left(1.96 \times 10^{-3}\ \text{m}^2\right), 0.001$ m, 5×10^{-4} kg, 1 kg/m^3, 100 s, 100 s, and 0.05 m, respectively. The volume of cylindrical pre-inlet reservoir V is set as zero for the comparison sake. These values have been partially adjusted from the estimates presented in the works of Liang et al. (2018) and Li et al. (2009). As seen in Fig. 2(a), increasing the value of τ_C leads to a higher maximum concentration and a shift of the peak to the right. On the other hand, increasing τ_J causes a decrease in the concentration peak and shifts the peak to the left. In Fig. 2(b), we can see that increasing τ_J results in a steeper slope of the breakthrough curve, while increasing τ_C leads to a flatter curve. Overall, these findings demonstrate the importance of considering the time lag effects in the classical ADE.

According to the definitions of τ_C and τ_J, τ_C is the result of microstructural interaction due to sorption or secondary pore water transfer, while τ_J is the result of inertial effects due to particle collision. In the cases of Fig. 2(a), the observation that a greater τ_J leads to higher concentration values at early times can be attributed to the fact that the injected mass particles collide near the inlet, resulting in some particles being pushed forward. On the other hand, a large value of τ_C indicates a stronger interaction between the mass particles and the soil resistance due to structural interaction. Initially, the injected mass particles stick to the soil due to sorption or secondary pore water transfer, resulting in low concentration values at early times. Later, the particles attached to the soil start to release, leading to a

large amount of mass being released into the flow path. This results in a higher peak in the intermediate period.

In contrast, Fig. 2 (b) shows that a higher τ_J leads to lower concentration values at early times and higher concentration values at late times. This is because the inertial force constantly exerts its effect on the continuously injected mass particles, leading to the particles being retained near the inlet for a while. A few times later, all of the particles with newly injected particles move toward the outlet, resulting in a higher concentration value at late times. Additionally, a greater τ_C leads to higher concentration values at early times and lower concentration values at late times. This is because the constantly injected mass particles are quickly released from the soil due to faster saturation of the soil pores compared to pulse injection. Later, the particles start to interact with the soil at late times. We can conclude that the effects of relaxation times show different results depending on the type of injection.

3.3. Sensitivity analysis results

Fig. 3 presents the sensitivity curves for both an instantaneous pulse and continuous injection. As seen in Eq. (6), the curves for R and n coincide due to their high correlation. The concentrations show high sensitivity to small changes in R, n, and q, followed by α, τ_J, and τ_C. The sensitivity curves in Fig. 3(a) change sign over time because of the instantaneous pulse, while only α, τ_J, and τ_C change sign in the case of continuous injection (Fig. 3(b)). These results indicate that R, n, and q can be determined with less uncertainty when identifying their values. While α has the second highest sensitivity, τ_J and τ_C show the least sensitivity, indicating when performing the parameter estimation, the estimates of τ_J, and τ_C may be determined with higher uncertainty levels. Therefore, a careful analysis of these two parameters in the inverse problem is needed.

3.4. Parameter estimation of column experiments

3.4.1. Case of instantaneous pulse—In Liang et al. (2018), four instantaneous pulse tracer tests were conducted on two soil columns, one containing coarse sand and the other containing finer sand. The columns had a length of 1.3 m and a diameter of 0.19 m . 0.33 L of chloride with a concentration of 1690 mg/L were used as a tracer and measured at distances of 0.35 and 0.8 m from the inlet. Data from test 1 (coarse sand) were used to test the proposed solution. The values of M and A were calculated as 5.58×10^{-4} kg and 0.028 m^2, respectively. The porosity of the sand was chosen as 0.37 on the basis of the estimate in Liang et al. (2018). The proposed solution and the Sauty (1980) solution were used to estimate the values of D (i.e.,) and v (i.e., q/n). The Sauty (1980) solution has the following expression:

$$C = \frac{M}{2nA\sqrt{D\pi t}} e^{-\frac{(x - vt)^2}{4Dt}}, \; x \in \left(-\infty, \infty \right) \tag{27}$$

It should be noted that the retardation factor R was assumed as unit for comparison. In addition, two statistical measures, the standard error estimate (SEE) and the mean error (ME), were used to evaluate the goodness-of-fit. The estimated results and the SEE and ME values are listed in Table 2.

Table 2 demonstrates that the proposed model produces lower values of SEE and ME for the two measured points compared to the solution provided by Sauty (1980). This is due to the fact that the proposed model has two additional relaxation times, making it more flexible and allowing for better fitting of the data. It should be noted that the SEE values already account for the effect of the number of degrees of freedom, indicating that the improved fitting results are not solely due to the additional parameters. Interestingly, the estimates of τ_C are greater than τ_c for both observed points. From the perspective of the threshold value θ, defined as $\tau_C/\tau_J, \theta$ reflects the significance of the relaxation times. If $\theta = 1$, the lag effects are insignificant; while $\theta > 1$ implies that τ_C dominates and $\theta < 1$ implies that τ_C governs the system. The θ values for the observations of 0.35 m and 0.8 m are 1.5(= 25,072.3 s/16,719.2 s) and 1.67(= 70,705.3 s/42,357.1 s), respectively. This indicates that τ_C plays a predominant role in solute transport behavior. The values of 1.5 and 1.67 imply the consistency of transport properties. Fig. 4 illustrates the BTCs predicted by the present solution and the solution provided by Sauty (1980), as well as the measured data from Liang et al. (2018). The curves predicted by the present solution align well with the measured data in comparison to the other solution.

3.4.2. Case of continuous injection—In a series of column experiments, Li et al. (2009) utilized two types of tracer, cesium (Cs) and tritium oxide (HTO), to study the transport of solutes in groundwater. The experiments were conducted under different operating conditions, and the primary material in the column was crushed granite. Data was collected at the outlet of the column at a distance of $x = 2$ cm(0.02 m) using a constant flow rate of $5\text{ml/min}\left(8.33 \times 10^{-8}\ \text{m}^3/\text{s}\right)$. The average flow velocity was calculated to be 4.24×10^{-5} m/s, and the inner diameter of the column was 5 cm (0.05 m). The concentration data was analyzed using the non-linear weight least squares method, and compared with the solution proposed by Ogata and Banks (1961), which is given by:

$$C = \frac{C_{in}}{2}\left[\text{erfc}\left(\frac{x - vt}{2\sqrt{Dt}}\right) + e^{\frac{vx}{D}}\text{erfc}\left(\frac{x + vt}{2\sqrt{Dt}}\right)\right],\ x \in \left(-\infty, \infty\right) \tag{28}$$

where $\text{erfc}(\cdot)$ is the complementary error function. More information on the experimental setup can be found in Fig. 2(b) of Li et al. (2009).

The estimated results and the SEE and ME values are listed in Table 3. The present solution again successfully fits the measured data, but here is for the case of continuous injection.

Fig. 5 presents the results of our fitting curves, which were predicted by our solution and the solution proposed by Ogata and Banks (1961), to the measured data. We observe that our solution shows good agreement with the data, with particular focus on the estimates of θ for Cs and HTO. These values are identified as 0.2 and 0.37 , respectively, and are less than

1 , indicating that τ_J plays a significant role in affecting solute transport. This finding is in contrast to our previous estimates from the experiment by Liang et al. (2018), where $\theta > 1$.

Using the definition of Peclet number $Pe = vx/D$, we can calculate Pe values from our experiments on instantaneous pulse (Table 2) and continuous injection (Table 3). In the case of instantaneous pulse, the Pe values for observations at 0.35 m and 0.8 m are 350 and 235.5 respectively. In the case of continuous injection, the Pe values for Cs and HTO are 0.8 and 5.89 respectively. These results show that the Pe values for the instantaneous pulse are significantly larger than those for continuous injection, leading to higher relaxation time estimates. This implies that increased advective transport increases the probability of particle collision and sorption in porous media.

Overall, our solution demonstrates superior performance in estimating transport parameters from BTC data compared to existing solutions. It serves as a useful tool for parameter estimation in situations where the BTC exhibits two-stage behavior.

4. Conclusions

In this study, we introduce the temporally relaxed theory into a mathematical model to describe the non-Fickian behavior of solute transport in one dimension. The concentration response is governed by an advection-dispersion equation that includes two relaxation times, τ_J and τ_c, which allow for differences in the timing of mass flux and concentration gradient. We compare our model with the MIM and RLS models and demonstrate that the relaxation times are equivalent to lumped parameters in these models (see Table 1). The use of relaxation times provides a new perspective for classifying solute transport, as exemplified by the threshold value $\theta = \tau_C/\tau_J$ (see Section 3.4).

The results of parameter estimation from column experiments indicate that our model fits well with the breakthrough curve from experiments by Liang et al. (2018) and Li et al. (2009). The estimates of θ also provide insight into the transport mechanisms of the solute; for example, the tests by Liang et al. (2018) show that the behavior is dominated by $\tau_C(\theta > 1)$, indicating resistance from structural interactions, while the tests by Li et al. (2009) show dominance of τ_J $(\theta < 1)$, indicating a strong inertial effect. In conclusion, the temporally relaxed theory provides more reliable estimates compared to existing advection-diffusion models, and offers a new approach to uncover physical insights in terms of relaxed times that are not otherwise evident in the past works. In future work, we plan to perform a numerical modeling analysis at the pore scale to investigate the relationship between pore-fluid interaction and relaxation times. Additionally, we will require additional experimental data, obtained through controlled tracer tests in the laboratory.

Acknowledgments

This research was supported by the grant from the Taiwan Ministry of Science and Technology under the contract number 110-2621-M002-012-MY3, from the Taiwan Water Resources Agency under the number 109-R-12-03-01-013-01-0, and from the Higher Education Sprout Project under the numbers 111L8807 and 111L890304. The data used to plot Figs. 4 and 5 are read from the works of Liang et al. (2018) and Li et al. (2009), respectively. The authors would like to extend their thanks to Elif Wong for her help with designing the

graphical abstract and to Dr. András Mészáros for providing the CME-S algorithm written in Mathematica script for numerical Laplace inversion.

Data availability

No data was used for the research described in the article.

Nomenclature

A	Cross-sectional area $\left[\mathrm{L}^2\right]$
(A_i, B_i)	Airy functions of first and second kinds
C	Concentration of solute $\left[\mathrm{ML}^{-3}\right]$
(C_m, C_{im})	Concentration of solute in mobile and immobile zones $\left[\mathrm{ML}^{-3}\right]$
C_0	Concentration of injection source $\left[\mathrm{ML}^{-3}\right]$
D	Dispersion coefficient $\left[\mathrm{L}^2\mathrm{T}^{-1}\right]$
D_0	Aqueous diffusion coefficient $\left[\mathrm{L}^2\mathrm{T}^{-1}\right]$
M	Total amount of solution used in the pulse injection [M]
J	Mass flux $\left[\mathrm{ML}^{-2}\mathrm{T}^{-1}\right]$
k_d	Partition coefficient of adsorption $\left[\mathrm{M}^{-3}\mathrm{L}\right]$
n	Porosity of media [-]
(n_m, n_{im})	Porosity of media in mobile and immobile zones [-]
O	Output of the model, i.e., $C\left[\mathrm{ML}^{-3}\right]$
Pe	Peclet number defined as vx/D
P_k k	th input parameter
q	Darcy flux $\left[\mathrm{LT}^{-1}\right]$
ΔP_k	$10^{-3}P_k$
R	Retardation factor [-]
(R_m, R_{im})	Retardation factor in mobile zone and immobile zone [-]
S	Mass amount in the solid phase [-]
s	Laplace parameter [-]

t	Time [T]
$\mathbf{V}$	Volume of the cylindrical pre-inlet reservoir $\left[\mathrm{L}^3\right]$
v	Seepage flow velocity $\left[\mathrm{LT}^{-1}\right]$
x	Distance from a source [L]
$\mathbf{X}$	Normalized sensitivity
α	Dispersivity [L]
$\beta\ n_m/n$	[-]
θ	Threshold value [-]
ρ_b	Bulk density of media $\left[\mathrm{ML}^{-3}\right]$
τ_0	Tortuosity [-]
(τ_J, τ_C)	Flux lagging and storage lagging, respectively [T]
(ω, ω^*)	First-order mass transfer coefficient for MIM and RLS models, respectively $\left[\mathrm{T}^{-1}\right]$

References

Addiscott TM, Whitmore AP, Powlson DS, et al., 1991. Farming, Fertilizers and the Nitrate Problem. CAB International (CABI).

Bedient PB, Rifai HS, Newell CJ, et al. , 1994. Ground Water Contamination: Transport and Remediation. Prentice-Hall International, Inc.

Benson DA, Meerschaert MM, Revielle J, 2013. Fractional calculus in hydrologic modeling: A numerical perspective. Adv. Water Resour 51, 479–497. 10.1016/j.advwatres.2012.04.005. [PubMed: 23524449]

Benson DA, Schumer R, Meerschaert MM, Wheatcraft SW, 2001. Fractional dispersion, Lévy motion, and the MADE tracer tests. Transp. Porous Media 42 (1), 211–240. 10.1023/A:1006733002131.

Benson DA, Tadjeran C, Meerschaert MM, Farnham I, Pohll G, 2004. Radial fractional-order dispersion through fractured rock. Water Resour. Res 40 (12), 10.1029/2004WR003314.

Benson DA, Wheatcraft SW, Meerschaert MM, 2000. The fractional-order governing equation of Lévy motion. Water Resour. Res 36 (6), 1413–1423. 10.1029/2000WR900032.

Berkowitz B, Cortis A, Dentz M, Scher H, 2006. Modeling non-Fickian transport in geological formations as a continuous time random walk. Rev. Geophys 44 (2), 10.1029/2005RG000178.

Berkowitz B, Emmanuel S, Scher H, 2008. Non-Fickian transport and multiple-rate mass transfer in porous media. Water Resour. Res 44 (3), W03402.

Berkowitz B, Klafter J, Metzler R, Scher H, 2002. Physical pictures of transport in heterogeneous media: Advection-dispersion, random-walk, and fractional derivative formulations. Water Resour. Res 38 (10), 9–1–9–12. 10.1029/2001WR001030.

Boano F, Packman A, Cortis A, Revelli R, Ridolfi L, 2007. A continuous time random walk approach to the stream transport of solutes. Water Resour. Res 43 (10), 10.1029/2007WR006062.

Bradford SA, Yates SR, Bettahar M, Simunek J, 2002. Physical factors affecting the transport and fate of colloids in saturated porous media. Water Resour. Res 38 (12), 63–1–63–12.

Brown GH, Brooks MC, Wood AL, Annable MD, Huang J, 2012. Aquitard contaminant storage and flux resulting from dense nonaqueous phase liquid source zone dissolution and remediation. Water Resour. Res 48 (6), 10.1029/2011WR011141.

Brusseau ML, Jessup RE, Rao PSC, 1991. Nonequilibrium sorption of organic chemicals: Elucidation of rate-limiting processes. Environ. Sci. Technol 25 (1), 134–142. 10.1021/es00013a015.

Carr EJ, 2020. New semi-analytical solutions for advection-dispersion equations in multilayer porous media. Transp. Porous Media 135 (1), 39–58. 10.1007/s11242-020-01468-z.

Carr EJ, 2021. Generalized semi-analytical solution for coupled multispecies advection-dispersion equations in multilayer porous media. Appl. Math. Model 94, 87–97. 10.1016/j.apm.2021.01.013.

Carr EJ, Turner IW, 2016. A semi-analytical solution for multilayer diffusion in a composite medium consisting of a large number of layers. Appl. Math. Model 40 (15–16), 7034–7050. 10.1016/j.apm.2016.02.041.

Chen JS, Ho YC, Liang CP, Wang SW, Liu CW, 2019. Semi-analytical model for coupled multispecies advective-dispersive transport subject to rate-limited sorption. J. Hydrol 579, 124164. 10.1016/j.jhydrol.2019.124164.

Chen K, Zhan H, Yang Q, 2017. Fractional models simulating non-Fickian behavior in four-stage single-well push-pull tests. Water Resour. Res 53 (11), 9528–9545. 10.1002/2017WR021411.

Dellóca A, Riva M, Guadagnini A, 2020. Global sensitivity analysis for multiple interpretive models with uncertain parameters. Water Resour. Res 56 (2), 10.1029/2019WR025754, e2019WR025754.

Dentz M, Berkowitz B, 2003. Transport behavior of a passive solute in continuous time random walks and multirate mass transfer. Water Resour. Res 39 (5), 10.1029/2001WR001163.

Dentz M, Cortis A, Scher H, Berkowitz B, 2004. Time behavior of solute transport in heterogeneous media: transition from anomalous to normal transport. Adv. Water Resour 27 (2), 155–173. 10.1016/j.advwatres.2003.11.002.

Dracos T, 1987. Immiscible transport of hydrocarbons infiltrating in unconfined aquifers. In: Oil in Freshwater: Chemistry, Biology, Countermeasure Technology. Elsevier, pp. 161–175.

Dubner H, Abate J, 1968. Numerical inversion of Laplace transforms by relating them to the finite Fourier cosine transform. J. ACM 15 (1), 115–123.

Edery Y, Guadagnini A, Scher H, Berkowitz B, 2014. Origins of anomalous transport in heterogeneous media: Structural and dynamic controls. Water Resour. Res 50 (2), 1490–1505. 10.1002/2013WR015111.

Elimelech M, O'Melia CR, 1990. Kinetics of deposition of colloidal particles in porous media. Environ. Sci. Technol 24 (10), 1528–1536.

Gao G, Zhan H, Feng S, Fu B, Ma Y, Huang G, 2010. A new mobile-immobile model for reactive solute transport with scale-dependent dispersion. Water Resour. Res 46 (8), 10.1029/2009WR008707.

Gaver DP Jr., 1966. Observing stochastic processes, and approximate transform inversion. Oper. Res 14 (3), 444–459.

Gerke HH, Van Genuchten MT, 1993. A dual-porosity model for simulating the preferential movement of water and solutes in structured porous media. Water Resour. Res 29 (2), 305–319. 10.1029/92WR02339.

Haggerty R, Gorelick SM, 1995. Multiple-rate mass transfer for modeling diffusion and surface reactions in media with pore-scale heterogeneity. Water Resour. Res 31 (10), 2383–2400. 10.1029/95WR10583.

Haggerty R, McKenna SA, Meigs LC, 2000. On the late-time behavior of tracer test breakthrough curves. Water Resour. Res 36 (12), 3467–3479. 10.1029/2000WR900214.

Hillel D, 2003. Introduction to Environmental Soil Physics. Elsevier.

Horváth G, Horváth I, Almousa SAD, Telek M, 2020. Numerical inverse Laplace transformation using concentrated matrix exponential distributions. Perform. Eval 137, 102067. 10.1016/j.peva.2019.102067.

Horváth I, Mészáros A, Telek M, 2023. Numerical inverse Laplace transformation beyond the Abate-Whitt framework. J. Comput. Appl. Math 418, 114651.

Huang J, Christ JA, Goltz MN, 2010. Analytical solutions for efficient interpretation of single-well push-pull tracer tests. Water Resour. Res 46 (8), 10.1029/2008WR007647.

Huang J, Goltz MN, 2015. Semianalytical solutions for transport in aquifer and fractured clay matrix system. Water Resour. Res 51 (9), 7218–7237. 10.1002/2014WR016073.

Kabala Z, 2001. Sensitivity analysis of a pumping test on a well with wellbore storage and skin. Adv. Water Resour 24 (5), 483–504. 10.1016/S03091708(00)00051-8.

Kelly JF, Bolster D, Meerschaert MM, Drummond JD, Packman AI, 2017. FracFit: A robust parameter estimation tool for fractional calculus models. Water Resour. Res 53 (3), 2559–2567. 10.1002/2016WR019748.

Kelly JF, Meerschaert MM, 2017. Space-time duality for the fractional advectiondispersion equation. Water Resour. Res 53 (4), 3464–3475. 10.1002/2016WR019668.

Knabe D, Guadagnini A, Riva M, Engelhardt I, 2021. Uncertainty analysis and identification of key parameters controlling bacteria transport within a riverbank filtration scenario. Water Resour. Res 57 (4), 10.1029/2020WR027911, e2020WR027911.

Li MH, Wang TH, Teng SP, 2009. Experimental and numerical investigations of effect of column length on retardation factor determination: a case study of cesium transport in crushed granite. J. Hard Mater 162 (1), 530–535. 10.1016/j.jhazmat.2008.05.076.

Li X, Wen Z, Zhan H, Wu F, Zhu Q, 2021. Laboratory observations for twodimensional solute transport in an aquifer-aquitard system. Environ. Sci. Pollut. Res 28 (29), 38664–38678. 10.1007/s11356-021-13123-1.

Liang X, Zhan H, Liu J, Dong G, Zhang YK, 2018. A simple method of transport parameter estimation for slug injecting tracer tests in porous media. Sci. Total Environ 644, 1536–1546. 10.1016/j.scitotenv.2018.06.330. [PubMed: 30743867]

Lin YC, Huang CS, Yeh HD, 2019. Analysis of unconfined flow induced by constant rate pumping based on the lagging theory. Water Resour. Res 55 (5), 3925–3940. 10.1029/2018WR023893.

Lin YC, Yeh HD, 2017. A lagging model for describing drawdown induced by a constant-rate pumping in a leaky confined aquifer. Water Resour. Res 53 (10), 8500–8511. 10.1002/2017WR021115.

Liou TS, Yeh HD, 1997. Conditional expectation for evaluation of risk groundwater flow and solute transport: one-dimensional analysis. J. Hydrol 199 (3–4), 378–402. 10.1016/S0022-1694(97)00025-5.

Malama B, Kuhlman KL, James SC, 2013. Core-scale solute transport model selection using Monte Carlo analysis. Water Resour. Res 49 (6), 3133–3147. 10.1002/wrcr.20273.

McDowell-Boyer LM, Hunt JR, Sitar N, 1986. Particle transport through porous media. Water Resour. Res 22 (13), 1901–1921.

Miiler R, 1996. Biological processes affecting contaminant fate and transport. Pollut. Sci. 77–91.

Ogata A, Banks RB, 1961. A Solution of the Differential Equation of Longitudinal Dispersion in Porous Media: Fluid Movement in Earth Materials. US Government Printing Office.

Ogolo NA, Onyekonwu M, 2022. Review of particle detachment and attachment in porous media. J. Appl. Sci. Process Eng 9 (2), 1209–1222.

Oliveira R, Bijeljic B, Blunt MJ, Colbourne A, Sederman AJ, Mantle MD, Gladden LF, 2021. A continuous time random walk method to predict dissolution in porous media based on validation of experimental NMR data. Adv. Water Resour 149, 103847. 10.1016/j.advwatres.2021.103847.

Panfilov M, Panfilova I, Stepanyants Y, 2008. Mechanisms of particle transport acceleration in porous media. Transp. Porous Media 74, 49–71.

Povstenko Y, 2015. Linear Fractional Diffusion-Wave Equation for Scientists and Engineers. Springer.

Rezaei A, Zare M, Zhan H, 2016. Aquitard horizontal dispersion on reactive solute transport in an aquifer-aquitard system. Transp. Porous Media 113 (3), 695–716. 10.1007/s11242-016-0719-6.

Sauty JP, 1980. An analysis of hydrodispersive transfer in aquifers. Water Resour. Res 16 (1), 145–158. 10.1029/WR016i001p00145.

Schumer R, Benson DA, Meerschaert MM, Baeumer B, 2003. Multiscaling fractional advection-dispersion equations and their solutions. Water Resour. Res 39 (1), 10.1029/2001WR001229.

Shi W, Wang Q, Salihu Danlami M, 2022. A novel analytical model of solute transport in a layered aquifer system with mixing processes in the reservoirs. Environ. Sci. Pollut. Res 29 (45), 67953–67968.

Stehfest H, 1970. Algorithm 368: Numerical inversion of Laplace transforms [D5]. Commun. ACM 13 (1), 47–49.

Trefethen LN, Weideman JAC, Schmelzer T, 2006. Talbot quadratures and rational approximations. BIT Numer. Math 46 (3), 653–670. 10.1007/s10543-006-0077-9.

Tzou DY, 1995. The generalized lagging response in small-scale and high-rate heating. Int. J. Heat Mass Transfer 38 (17), 3231–3240. 10.1016/00179310(95)00052-B.

Tzou DY, Özişik MN, Chiffelle R, 1994. The lattice temperature in the microscopic two-step model. J. Heat Transfer 10.1115/1.2911439.

Van Genuchten MT, Wagenet R, 1989. Two-site/two-region models for pesticide transport and degradation: Theoretical development and analytical solutions. Soil Sci. Am. J 53 (5), 1303–1310. 10.1029/2019WR025697.

Wang Q, Gu H, Zhan H, Shi W, Zhou R, 2020. Mixing effect on reactive transport in a column with scale dependent dispersion. J. Hydrol 582, 124494.

Wood JA, Anthony DH, 1997. Herbicide contamination of prairie springs at ultratrace levels of detection. Technical Report, Wiley Online Library.

Yang Y, Yuan W, Hou J, You Z, 2022. Review on physical and chemical factors affecting fines migration in porous media. Water Res. 118172.

Zhang Y, Benson DA, Meerschaert MM, LaBolle EM, 2007. Space-fractional advection-dispersion equations with variable parameters: Diverse formulas, numerical solutions, and application to the Macrodispersion Experiment site data. Water Resour. Res 43 (5), 10.1029/2006WR004912.

Zhang Y, Benson DA, Reeves DM, 2009. Time and space nonlocalities underlying fractional-derivative models: Distinction and literature review of field applications. Adv. Water Resour 32 (4), 561–581. 10.1016/j.advwatres.2009.01.008.

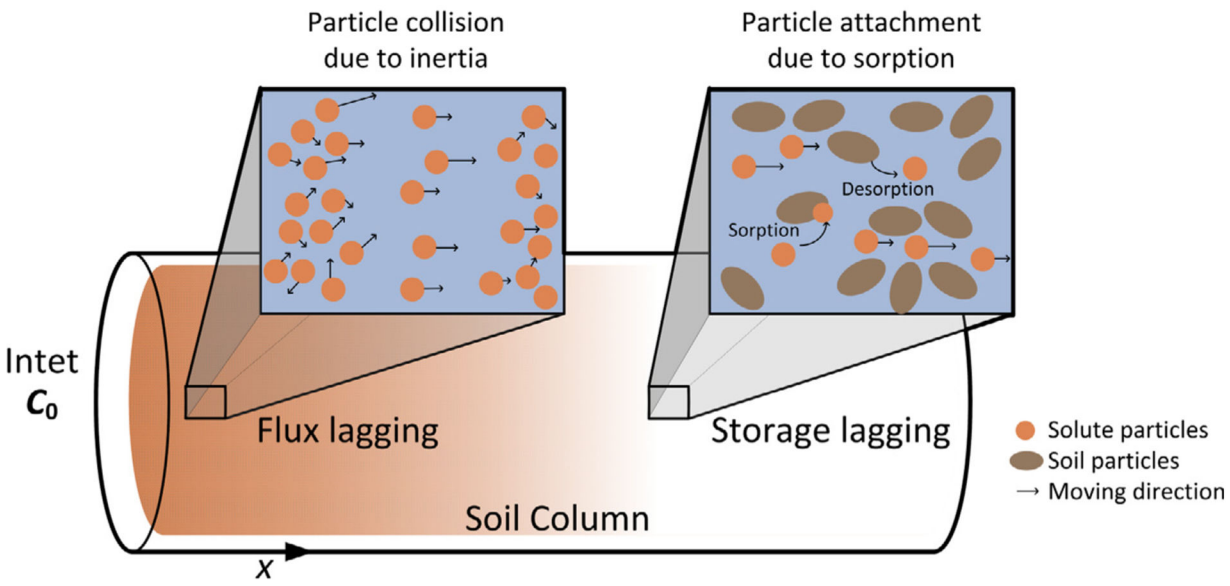

Fig. 1.

Schematic diagram of the one-dimensional solute transport in the soils affected by the temporally relaxed effects due to inertial force and sorption.

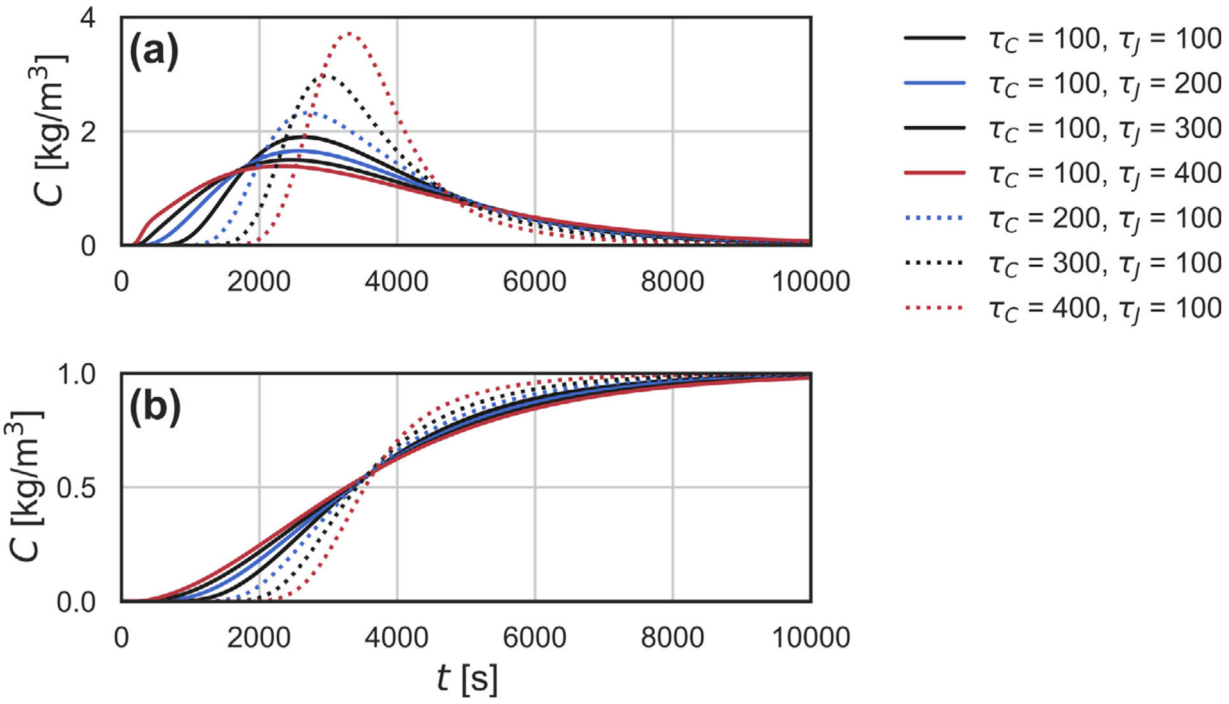

Fig. 2.

The temporal concentration distribution predicted by (a) instantaneous pulse and (b) continuous injection with various τ_J and τ_C.

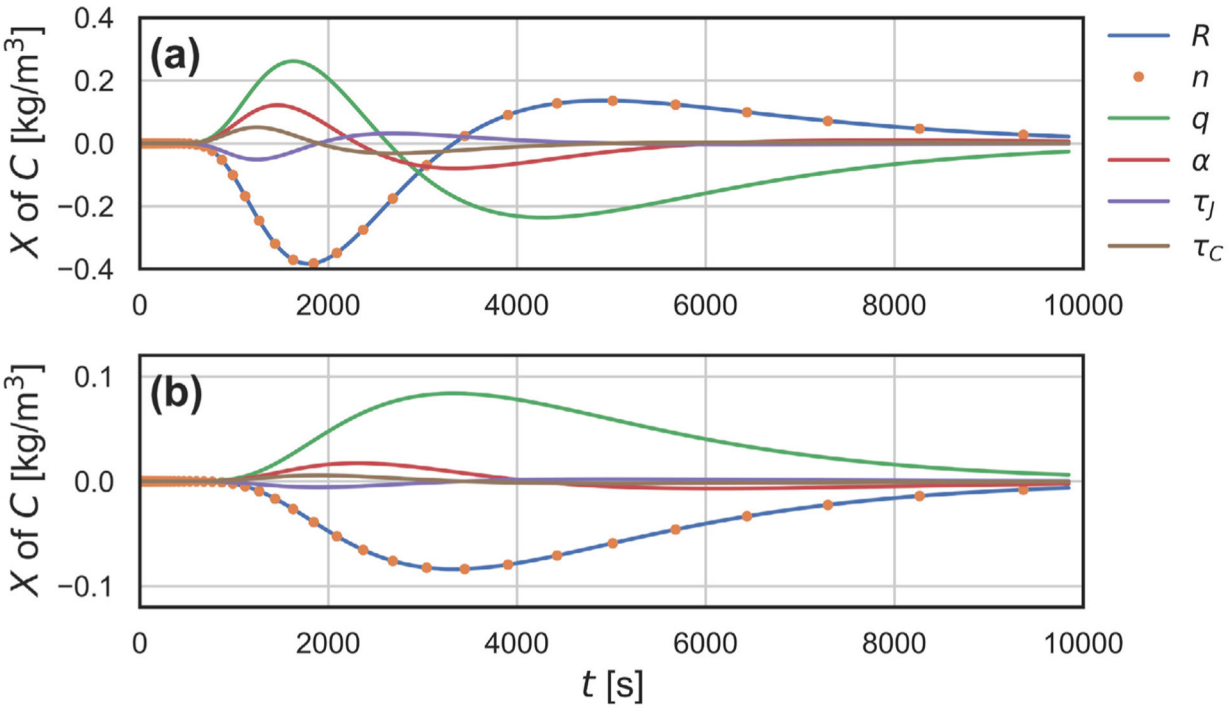

Fig. 3.
The sensitivity analysis results for (a) instantaneous pulse and (b) continuous injection.

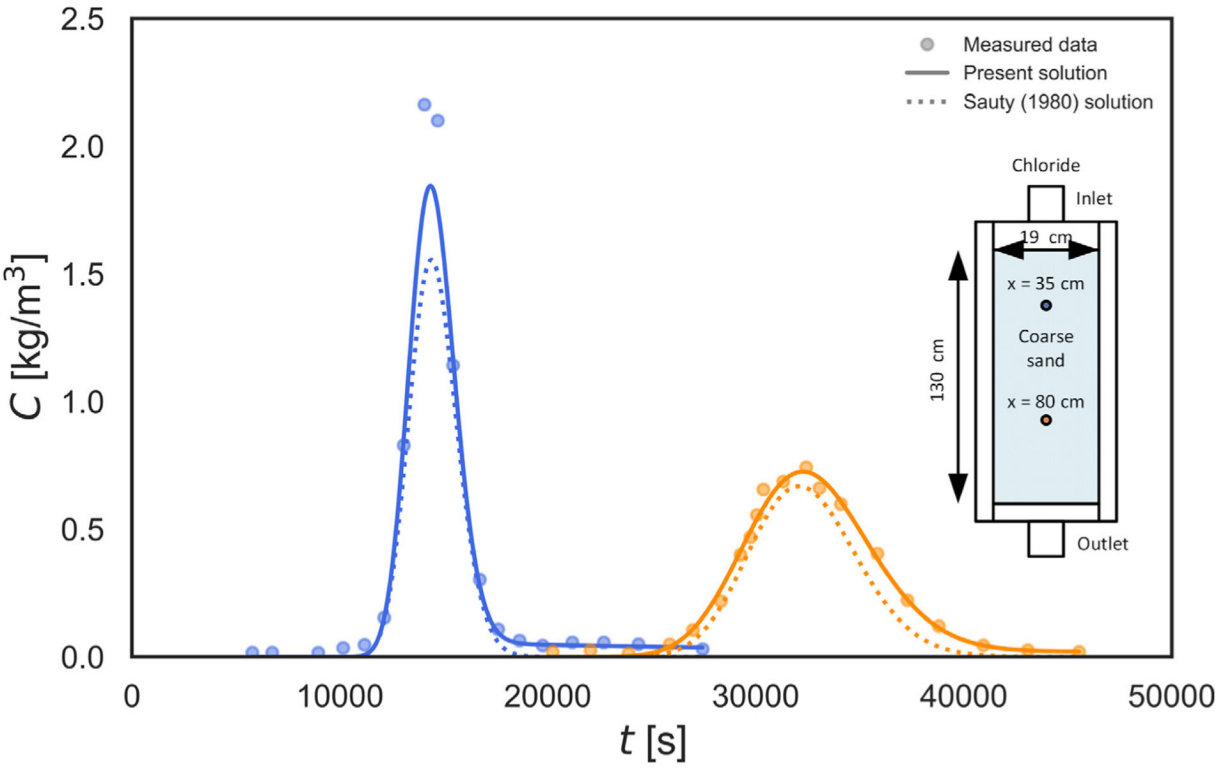

Fig. 4.

The concentration curves predicted by present and Sauty (1980) solutions and the measured data of chloride observed at 0.35 m and 0.8 m from the inlet from the test of Liang et al. (2018).

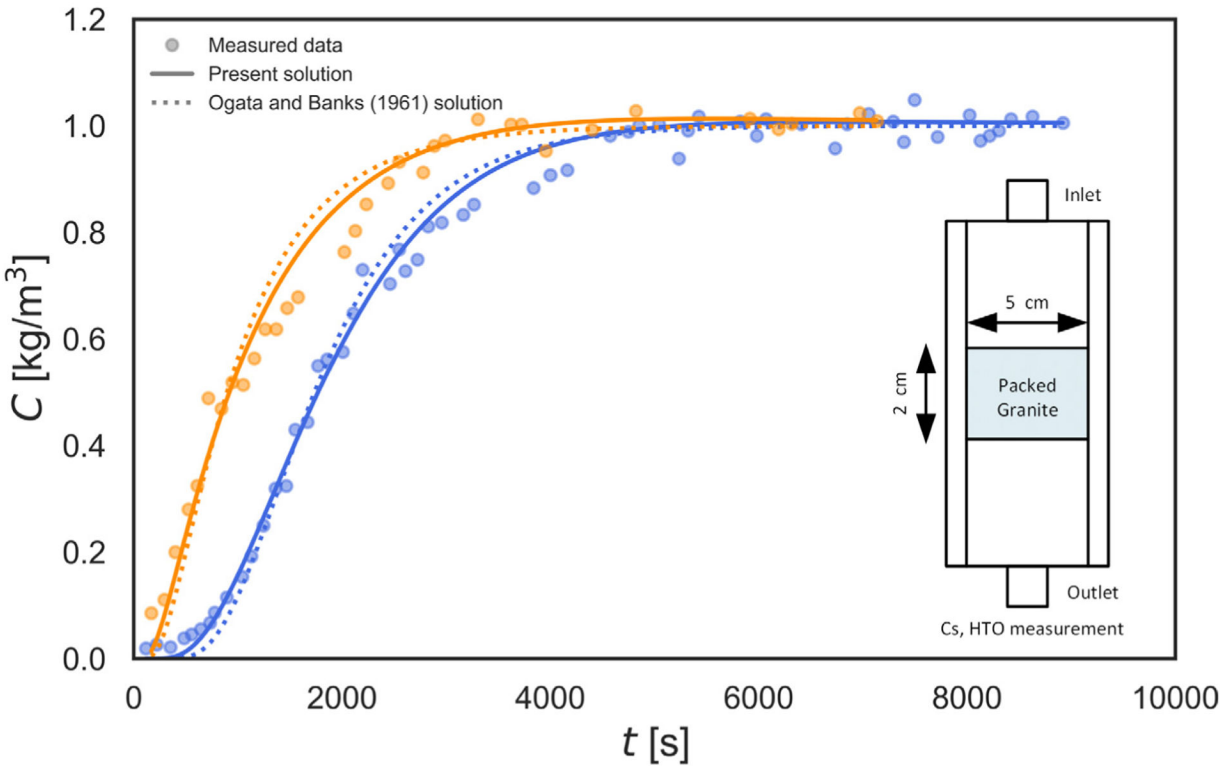

Fig. 5.

The concentration curves predicted by present and Ogata and Banks (1961) solutions and the measured data of Cs and HTO from the test of Li et al. (2009).

Table 1

Comparison of the present model and the MIM and RLS models.

Present model	MIM model	RLS model
$R =$	$\frac{n_m}{n}R_m + \frac{n_{im}}{n}R_{im}$	$1 + \frac{\rho_b k_d}{n}$
$\tau_J =$	$\frac{n_m R_m n_{im} R_{im}}{\omega(n_m R_m + n_{im} R_{im})}$	$\frac{1}{\omega^*}\left(1 + \frac{\rho_b k_d}{n}\right)^{-1}$
$\tau_C =$	$\frac{n_{im} R_{im}}{\omega}$	$\frac{1}{\omega^*}$

Table 2

Results of parameter estimation for column experiments from Liang et al. (2018).

Solution	D (m^2/s)	v (m/s)	τ_f (s)	τ_c (s)	θ	SEE (kg/m^3)	ME (kg/m^3)
Observed at 0.35 m							
Present solution	1.61×10^{-8}	1.61×10^{-5}	16719.2	25072.3	1.50	0.140	0.048
Sauty (1980)	2.60×10^{-8}	2.41×10^{-5}	-	-	-	0.248	0.112
Observed at 0.8 m							
Present solution	4.96×10^{-8}	1.46×10^{-5}	42357.1	70705.3	1.67	0.027	0.03
Sauty (1980)	6.31×10^{-8}	2.47×10^{-5}	-	–	–	0.073	0.058

Table 3

Results of parameter estimation for column experiments from Li et al. (2009).

Solution	D (m^2/s)	v (m/s)	τ_f (s)	τ_C (s)	θ	SEE (kg/m^3)	ME (kg/m^3)
Cesium, Cs							
Present solution	4.68×10^{-7}	1.88×10^{-5}	2926.0	578.1	0.20	0.031	−0.007
Ogata and Banks (1961)	2.84×10^{-8}	1.16×10^{-5}	-	-	-	0.038	−0.006
Tritium oxide, HTO							
Present solution	4.96×10^{-8}	1.46×10^{-5}	2337.9	865.2	0.37	0.048	−0.011
Ogata and Banks (1961)	1.38×10^{-7}	2.33×10^{-5}	–	–	–	0.064	−0.012